IEEE Access
Multidisciplinary ⋮ Rapid Review ⋮ Open Access Journal

Received February 6, 2020, accepted February 28, 2020, date of publication March 5, 2020, date of current version March 16, 2020.

Digital Object Identifier 10.1109/ACCESS.2020.2978754

PartMitosis: A Partially Supervised Deep Learning Framework for Mitosis Detection in Breast Cancer Histopathology Images

MERIEM SEBAI[1], **TIANJIANG WANG**[1], **AND SAAD ALI AL-FADHLI**[1,2]
[1]School of Computer Science and Technology, Huazhong University of Science and Technology (HUST), Wuhan 430074, China
[2]Department of Computer Techniques Engineering, Imam Al-Kadhum College (IKC), Baghdad 10001, Iraq

Corresponding authors: Meriem Sebai (meriemsebai@hust.edu.cn) and Tianjiang Wang (tjwang@hust.edu.cn)

ABSTRACT Detection of mitotic tumor cells per tissue area is one of the critical markers of breast cancer prognosis. The aim of this paper is to develop a method for the automatic detection of mitotic figures from breast cancer histological slides using a partially supervised deep learning framework. Unlike the previous literature, which has focused on solving the problem of mitosis detection in the weakly annotated datasets using centroid pixel labels (weak labels) only without taking advantage of the available pixel-level labels (strong labels) of other datasets, in this paper, we design a novel partially supervised framework based on two parallel deep fully convolutional networks. One of them is trained using weak labels and the other is trained using strong labels, together with a weight transfer function. In the detection phase, we fuse the segmentation maps produced by the two networks to obtain the final mitosis detections. Our system exploits the available large sets of mitosis detection samples with mitosis centroid annotation, such as the 2014 ICPR dataset and the AMIDA13 dataset, and only a small set of samples with the annotation of all mitosis pixels, such as the 2012 ICPR dataset, to perform a more accurate mitosis detection on weakly labeled data. This enables us to outperform all previous mitosis detection systems by achieving F-scores of 0.575 and 0.698 on the 2014 ICPR dataset and the AMIDA13 dataset respectively.

INDEX TERMS Mitosis detection, partially supervised learning, breast cancer grading, fully convolutional network, transfer learning.

I. INTRODUCTION

The most recommended breast cancer grading system by the World Health Organization (WHO), is the Nottingham grading system [1]. It involves three biomarkers: tubule formation, nuclear pleomorphism score, and mitosis (i.e., cell in the process of nuclear division) counting. Because the spread of cancer is highly related to cellular divisions, detecting the mitotic cells in histopathology images and counting them is the most important indicator for assessing the risk of metastasis. Clinically, the breast biopsied tissue specimens are fixed by paraffin and stained with Hematoxylin and Eosin (H&E) dyes. After acquiring the images of these stained blocks, histology slide images are obtained. In general, pathology experts manually mark the mitotic cells on High Power Fields (HPFs), which are microscopic observations with 40x magnification. However, the manual annotation of mitoses is a very time-consuming task since a single Whole Slide Image (WSI) may contain a large number of HPFs. Besides, due to the high biological variation of mitotic cells, manual detection is usually prone to error. Therefore, automating this process is extremely essential for reducing the time spent annotating and the labour employed in pathology laboratories. The detection of mitoses from histological stained slides is quite challenging. In fact, the configurations of the shape and texture of the cells in the different growth stages of mitosis (prophase, metaphase, anaphase, and telophase) are varied. For instance, in the telophase stage, a nucleus has two distinct parts that have to be considered as one cell since they are not yet fully divided. Besides, there are many mimic cells (such as lymphocytes, apoptotic cells, dense nuclei) which are extremely similar to mitoses in appearance, making it hard for the detection process to deal with false positives. Moreover, there is a diversity of tissue appearance in histopathology slides, due to the different conditions of preparation and acquisition.

The associate editor coordinating the review of this manuscript and approving it for publication was K. C. Santosh.

In recent years, many mitosis detection contests have been organized, including the 2012 ICPR MITOSIS contest [2], the 2014 ICPR MITOSIS-ATYPIA challenge [3] and the AMIDA13 contest [4]. Thus, many publications have been dedicated to solving the problem of mitosis detection from H&E stained images.

The early proposed approaches [5]–[12] use manually designed features, such as morphological, statistical and textural features to describe the mitosis appearance. However, because of the diversity of the shapes of the mitosis and the high similarity between mitotic and non-mitotic cells, it is very arduous to define hand-crafted features that can well discriminate mitoses from mimics.

Another category of features used to address this medical problem is the category of convolutional features [13]–[22]. The advantage of features based on Convolutional Neural Networks (CNNs) is their ability to capture automatically the characteristics of the appearance of mitotic cells. Current approaches based on CNNs typically address the problem of mitosis detection in two different ways: (1) Fully supervised. E.g., [16] propose detecting mitotic cells using a deep regression network based on a Fully Convolutional Network (FCN). A local maximum of the output score map is considered to be the centroid of a mitosis. [20] apply the region-based deep detection network Faster RCNN for mitosis detection. The detected mitosis candidates are further classified using a deep verification network to improve the system's performance. The principal drawback of these methods is that they require full supervision, which is expensive since the annotation of every mitotic pixel in the HPFs is very labour intensive. In contrast, mitosis centroids are much easier to mark, which is why the weakly annotated data is more abundant. (2) Weakly supervised. E.g., [20] propose a solution to address the problem of training their region-based deep detection network in a weakly supervised way, by estimating the mitosis bounding box labels for the weakly annotated dataset using an FCN as a deep segmentation network. The drawback of this method is that the FCN fails to generate reliable bounding box annotations, which reduces the performance of the detector by introducing inaccurate supervision during the training. Reference [22] consider the problem of mitosis counting as a semantic segmentation task. Since the training of a semantic segmentation network such as an FCN requires pixel-level annotations, to deal with mitosis centroid-pixel labels, they introduce a novel kind of annotation, referred to as the concentric label. Associated with this weak label, a weak loss function, referred to as the concentric loss, is also defined. This method achieves state-of-the-art performance on the 2014 ICPR MITOSIS dataset and the AMIDA13 dataset with F-scores of 0.562 and 0.672 respectively.

With the availability of two different types of annotations in mitosis benchmarks, centroid-pixel annotations and pixel-level annotations, a key question can be raised: Is it possible to train a mitosis detection model using both strong and weak labels? With this motivation, in the present paper we introduce a novel method based on partially supervised semantic segmentation for mitosis detection from histopathological slide images.

We formulate the partially supervised semantic segmentation in the mitosis detection task as follows: there are given two types of datasets, one dataset with the annotation of all pixels of each mitosis, and the other dataset with the annotation of only the mitosis centroid pixels. Our mitosis detection algorithm should use this data to train a framework with two parallel semantic segmentation networks: the first using the data with weak labels (like the centroid labels), and the second using the data with pixel-level labels. These two networks are connected via a transfer weight function that enables the transfer of semantic information from the segmentation network trained with weak labels to the segmentation network trained with strong labels, and thus tackle the problem of training the strong segmentation network on a dataset without pixel-level annotations. The idea of using a weight transfer function as a kind of transfer learning technique was first introduced in [23] to train the instance segmentation network Mask R-CNN on a large set of classes that all have box annotations but only a small subset of which have instance masks.

The intuition behind this weight transfer function in our partially supervised mitosis detection framework is that once the model is trained, the parameters of the weak segmentation head encode an embedding of the image semantic segmentation but in a coarse way, since this part of the model is trained with weak labels. This embedding allows the transfer of coarse semantic information to the partially supervised pixel-wise segmentation head, which can segment the image in a finer way. This weight function is trained with the two segmentation networks in an end-to-end way. Since the training set comprises a large set of samples that all have weak annotations (centroid labels) but only a small subset of which have pixel-level labels (strong annotations), this task is considered as partially supervised. The final detection results are the weighted sum of the weak segmentation branch predictions and the strong segmentation branch predictions.

The major advantage of designing a partially supervised mitosis detection model is to exploit both types of available datasets, namely the datasets with pixel-level annotations, such as the 2012 ICPR MITOSIS dataset, for which we can also generate centroid annotations, and the datasets with only mitosis centroid-pixel annotations, such as the 2014 ICPR MITOSIS dataset and the AMIDA13 dataset.

To sum up, the present paper make three contributions: (1) We design a novel mitosis detection system that can be trained in a partially supervised way with a large weakly annotated mitosis dataset and a small fully labeled mitosis dataset and can achieve a highly accurate detection performance. As far as we know, this is the first paper that employs partially supervised learning to train a deep learning framework based on semantic segmentation for the more accurate detection of mitotic cells from weakly annotated datasets by taking advantage of the few available fully annotated mitosis

image samples. (2) We integrate a simple, easy to train weight transfer function into our system that allows the transfer of semantic knowledge from the semantic segmentation branch trained with weak labels to the semantic segmentation branch trained with strong labels. (3) We evaluate our method on several mitosis datasets that are provided by various pathology laboratories and conclude that our approach yields state-of-the-art detection performance on all of these benchmarks.

The rest of this paper is structured around 4 sections: Section. II presents the related literature. The proposed approach, as well as the description of the datasets used, are presented in Section. III. The experiments and results are presented in Section. IV. Some conclusions and perspectives for future research are presented in Section. V.

II. RELATED WORK

Following the adoption of scanners for WSI on microscope stained sections, much research on the automatic detection of mitoses from histopathological slides has been carried out. In terms of image features, mitosis detection approaches can be divided into two types: methods that employ hand-crafted features and methods that use Convolutional Network (ConvNet) features.

Hand-crafted based approaches were the first methods employed to tackle this medical problem [5]–[12]. These methods usually classify the mitosis candidates using different manually extracted features, such as morphological, textural, and statistical features. However, since the mitoses have varied shapes and textures, it is hard to manually define features that can effectively represent the mitotic cells.

The world of computer vision has been reborn since the introduction of convolutional neural networks by [24]. Methods based on CNNs have achieved state-of-the-art performance in many tasks, such as image classification [25]–[30], object detection [31]–[35], and semantic segmentation [36], [37]. In recent years, the field of medical image analysis has attracted the attention of many researchers [38]–[42]. Hence, several approaches based on deep CNNs have been proposed to tackle different medical tasks, for instance [41] develop a ConvNet based system for the classification of malignant and benign cells in breast cytology images, while [42] propose a two-stream attention based framework for organ segmentation. CNN based approaches are the other type of methods used to address the problem of detecting mitoses from histology images [13]–[22]. Reference [13] employ both hand-crafted and convolutional features to make the mitosis detection system more effective. Reference [14] propose a cascaded system that generates mitosis candidate patches and then classifies them using two separate classifiers, one based on hand-crafted features and the other one on CNN features. For those candidate patches that are difficult to classify, another classifier that combines both hand-crafted features and convolutional features is applied. IDSIA [15] train a deep neural network to classify image patches into mitosis and non-mitosis. However, at inference time, since the trained classifier is a pixel-classifier, it is applied using a sliding window, which makes the system computationally intensive. DRN [16] train a deep regression network built on FCN for mitosis detection. In the detection stage, the location of the centroid of the mitosis is inferred to be the local maximum. Though this method yields excellent performance in the fully annotated 2012 ICPR MITOSIS dataset, it can not be applied to a dataset without pixel-level annotations. CasNN [17] adopt a cascaded detection system that contains two CNNs. The first network is an FCN used to coarsely locate and retrieve the mitosis candidates. The second network is a classification network used to classify the candidate patches and screen out the mitosis' mimics. The drawback of this method is that its two networks are trained separately, which may be an impediment to the integration of the system. MFF-CNN [18] design a multi-scale fused CNN for mitosis detection. The model comprises two multi-scale branches that fuse features across different layers. The final detection is obtaining by combining the predictions of the two branches. In the training stage, the training samples, comprising mitotic and non-mitotic patches, are selected from the blue ratio images. In the detection stage, the trained model is converted to an FCN to detect the mitotic cells directly from the HPF image. MSSN [19] employ a two-stage deep learning framework for mitosis detection. In the first stage, a False Negative Reduction Model (FNRM) comprising 4 sub-networks is used to retrieve all possible mitosis candidates. Each sub-network exploits different contextual information to produce its output. Then the predictions of the 4 sub-models are combined. In the second stage, a False Positive Reduction Model (FPRM) which is a similarity prediction model is employed to get the final mitosis detections by filtering out the maximum number of false mitoses. This approach achieves promising results on the 2012 ICPR MITOSIS dataset and the 2014 ICPR MITOSIS dataset. DeepMitosis [20] propose a framework based on a general object detection network to detect the mitotic cells from H&E stained slides. Since an object detection network can only be applied to pixel-level annotated datasets, an FCN is used to segment the mitotic cells annotated only with the centroid-pixel. This method leads to an F–score of 0.832 on the fully annotated ICPR 2012 MITOSIS dataset, which outperforms all previous work. However, on the 2014 MITOSIS dataset, due to the weak supervision, this method is less efficient. Reference [21] propose an improved RCNN model for mitosis detection. As in the DeepMitosis approach, this method adopts an object detection network to address this medical task. A CNN is used to extract deep and shallow features from different level layers. These features are combined and fed into the Regional Proposal Network (RPN) to generate mitosis candidates. These candidates are then classified by the improved RCNN to produce the final detections. In addition to the object bounding box regressor, the improved RCNN employs two classification sub-networks that use different features selection methods to predict the object class. This method achieves a state-of-the art performance on the 2012 ICPR MITOSIS dataset, with an F-score of 0.851. However, like

the other object detection based methods, it can not be directly applied to a dataset with weak labels. SegMitos [22] use an FCN as a semantic segmentation model to segment and classify the mitotic cells. A concentric label and a concentric loss function are defined to train the FCN with the mitosis centroid-pixel annotated datasets. A concentric label comprises two circles: the area surrounded by the small circle is part of the mitotic cell, while the area outside the large circle is a non-mitotic region. The area of the annular region between the two circles contains both mitotic and non-mitotic parts. During the computation of the training loss, known as the concentric loss, the annular region is ignored since it is considered as a neutral area. This method achieves state-of-the-art performance on three different weakly annotated mitosis datasets.

Different convolutional neural networks have been used to address the problem of detecting mitoses from histopathological images, such as patch classification networks, detection networks, semantic segmentation networks, and deep regressors. Most of these networks are trained either in a fully supervised way or in a weakly supervised way. We note that no partially supervised deep learning framework has been employed to tackle this medical task. Therefore, in this paper, we introduce PartMitosis, a mitosis detection framework with: (1) Two semantic segmentation streams. The first stream is a segmentation network trained with weak labels and the second stream is another segmentation network trained with strong labels. (2) A weight transfer function that connects the two networks and transfers the semantic knowledge from the first branch to the second branch, and thus allows the prediction of the precise segmentation map (the map produced by the strong segmentation branch) for all images including those from the dataset without strong annotations in the training stage. PartMitosis is a partially supervised method that transfers semantic information from the model's weak predictors to its strong predictors through a weight transfer function and then fuses the scores of the two predictors for a more accurate mitosis detection from weakly labeled H&E stained slides.

III. APPROACH

A. DESCRIPTION OF THE DATASETS

1) ICPR 2012 MITOSIS DATASET

The ICPR 2012 dataset [2] contains 5 breast cancer biopsy slides from which 50 H&E stained images of size 2084×2084 pixels have been selected by pathologists. Each image represents a 512×512 μm^2 HPF generated by an Aperio XT scanner with a resolution of 0.2456 μm per pixel. According to the rules of the 2012 MITOSIS contest, 35 HPFs with 226 mitotic cells are used for training and 15 HPFs with 101 mitoses are used for evaluation. Since pathologists have provided an annotation of all mitosis pixels, this dataset is considered a strongly supervised dataset.

2) ICPR 2014 MITOSIS DATASET

The ICPR 2014 dataset [3] comprises 1200 HPFs used for training and 496 HPFs used for testing. Each HPF image has 1539×1376 pixels. There are 749 mitotic cells in the training data. Since the ground truth labels of the testing set were not released by the organizers, the number of mitoses is unknown. For this dataset, pathologists have provided the annotations only of the mitosis centroid pixels, hence, it is considered a weakly supervised dataset.

3) AMIDA13 DATASET

The Assessment of Mitosis Detection Algorithms 2013 (AMIDA13) challenge dataset [4] comprises 606 2000×2000 pixel HPF images. The training set comprises 311 HPFs obtained from 12 subjects. The testing set comprises 295 HPFs obtained from 11 subjects. The total number of mitotic cells in this dataset is 1083, of which 550 belong to the training set and 533 to the testing set. This dataset is also weakly supervised since the pathologists have annotated only the centroid pixels of the mitoses.

B. PARTMITOSIS MODEL

Fig. 1 illustrates the architecture of PartMitosis, the partially supervised mitosis detection framework. It uses two deep semantic segmentation networks; each of them is an FCN. An FCN [43] is a dense prediction ConvNet used for semantic segmentation in natural images. It extends a deep classification network to input images of arbitrary sizes, and outputs a segmentation map of the corresponding size by transforming the Fully Connected (FC) layers into convolution layers followed by an up-sampling layer. The FCN is pre-trained using image classification and then fully convolutionally fine-tuned for a fast dense learning and accurate dense prediction.

An FCN is the most suitable semantic segmentation network for our PartMitosis system for many reasons: (1) Due to the simple structure of an FCN, we can easily fit two streams of FCNs into our GPU without occupying too much memory. (2) The integration of the weight transfer function into our system that uses two streams of FCNs is very simple and straightforward. (3) The FCN is a semantic segmentation network that can achieve an excellent trade-off between accuracy and speed. (4) The FCN is a simple yet effective deep learning network originally designed for semantic segmentation in natural images. Much previous research has shown the advantages of knowledge transfer from the domain of natural images to the domain of medical images [44]. Hence, we propose using an FCN model pretrained on natural images as our initial model and fine-tuning it on the mitosis detection datasets to achieve highly accurate segmentation performance.

Let C be the set of training data that we use to train our PartMitosis model. The existing methods presume that all training samples in C are annotated either with a mitosis centroid pixel label (Fig. 2.(a)) or with a pixel-level

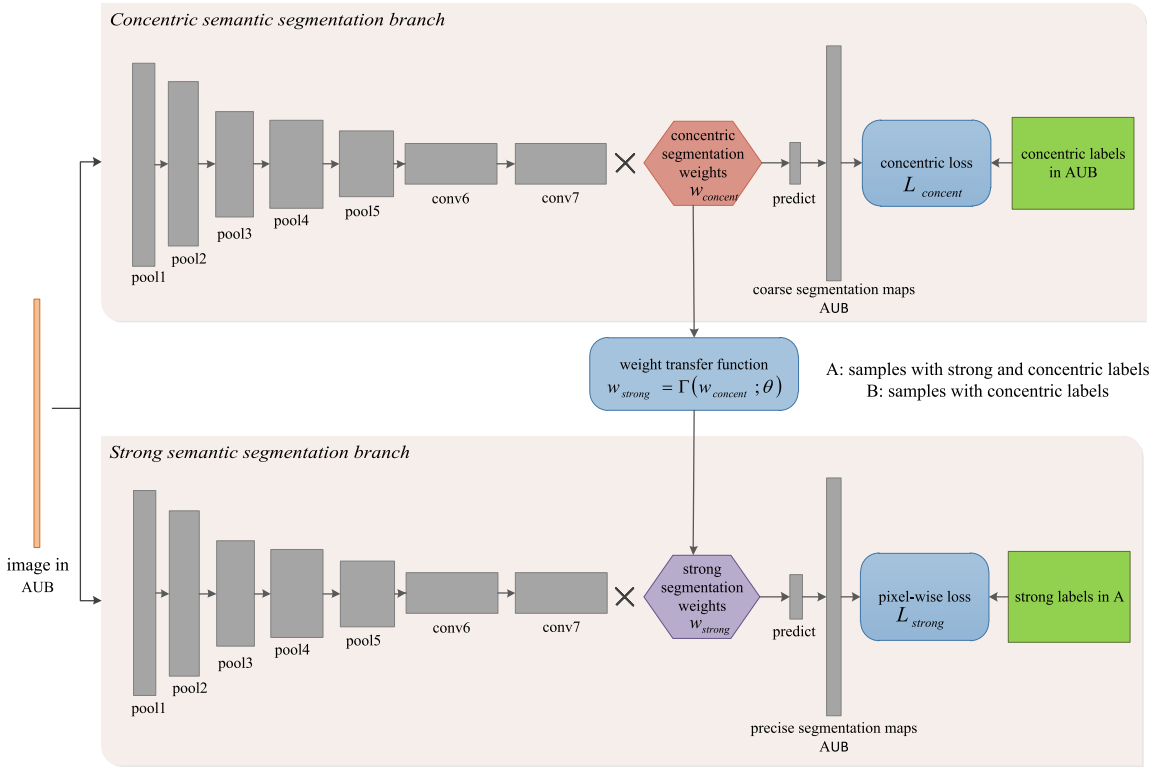

FIGURE 1. **Detailed overview of the PartMitosis system. The weights of the prediction layer of the strong segmentation branch W_{strong} are predicted from the weights of the prediction layer of the concentric segmentation branch $W_{concent}$ by means of a weight transfer function Γ and are not learned as model parameters. In the training stage, the strong segmentation branch and the weight transfer function Γ receive the gradient from the pixel-wise loss computed on set A only, while in the testing stage, the precise segmentation map can be predicted for all images in set $A \cup B$.**

label (Fig. 2.(b)). We presume that $C = A \cup B$, where samples from the set A have pixel-level labels and thus also have centroid-pixel labels (since we can easily extract a centroid label from pixel-level labels), while samples from the set B have only centroid pixel labels.

The 2012 MITOSIS dataset is strongly supervised while the 2014 ICPR MITOSIS dataset and the AMIDA13 dataset are weakly supervised. Since the training of PartMitosis requires both types of mitosis annotations (pixel-level and centroid-pixel), for each weakly annotated dataset we train a PartMitosis model using the weak labels of this dataset as well as the strong and weak labels of the 2012 MITOSIS dataset. For instance, to train a PartMitosis model for mitosis detection in the 2014 ICPR MITOSIS dataset, we use the samples of this dataset as set B and use the samples of the 2012 MITOSIS dataset as set A.

The first semantic segmentation network is the weak segmentation network that we called the concentric segmentation network. It is trained using the samples from the centroid-pixel annotated dataset B and the samples from the pixel-level annotated dataset A after converting the pixel-level labels into centroid-pixel labels. Since a centroid label is inappropriate for training a deep segmentation network because it does not provide any information about the morphological appearance of the mitosis, we propose transforming the centroid-pixel

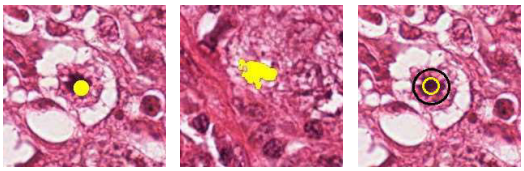

FIGURE 2. **Examples of labels. (a) Centroid-pixel label of a mitosis. (b) Pixel-level label of a mitosis. (c) Concentric label of a mitosis. The area surrounded by the yellow circle contains mitosis pixels only, while the annular area between the black and yellow circles contains both mitotic and non-mitotic pixels.**

label of a mitosis into a concentric label [22], i.e., around each mitosis centroid, we define two circles, as illustrated in Fig. 2.(c). We make the small circle (the circle in yellow in Fig. 2.(c)) so that all pixels inside of it belong to the mitotic cell, hence all these pixels will have a mitotic (positive) label. We make the large circle (the circle in black in Fig. 2.(c)) so that all pixels outside of it belong to the background, thus all these pixels will have a non-mitotic (negative) label. Since a mitotic cell has an average area of 590 pixels [22], the radius of the small circle r is randomly selected from a uniform distribution within the interval [10, 17], and the radius of the large circle R is randomly equal to 1.5 times to 2.5 times the radius of the small circle. The small circle is surrounded

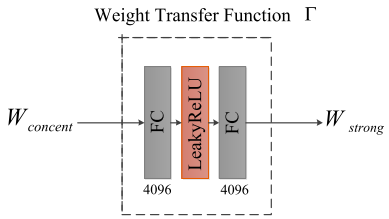

FIGURE 3. Illustration of the weight transfer function Γ.

by an annular region known as the 'middle ground'. The middle ground is regarded as a neutral region since some of its pixels belong to the mitotic cell but some others are not mitotic pixels. The concentric semantic segmentation branch is trained with the concentric loss function [22], a pixel-wise Softmax loss function for which the pixels contained in the annular region do not participate in its computation.

The second semantic segmentation network, referred to as the strong segmentation network, is trained with the pixel-wise Softmax loss function using the pixel-level labels of the fully annotated dataset A.

Since the last convolutional layer of the concentric segmentation network and the last convolutional layer of the strong segmentation network both contain semantic parameters, we propose predicting the semantic parameters of the strong segmentation branch from the semantic parameters of the concentric segmentation branch rather than training them separately. This kind of transfer learning is performed through a semantic weight transfer function. The whole system, which comprises the two segmentation networks and the weight transfer function, is trained jointly in an end-to-end manner.

Let $W_{concent}$ be the weights of the last convolutional layer (the layer before the up-sampling) of the fully convolutional network trained with the concentric labels, and let W_{strong} be the weights of the last convolutional layer of the FCN trained with the strong labels. A weight prediction function $\Gamma(.)$ is used to parametrize W_{strong}, rather than considering W_{strong} as the model's parameters (see Eq. (1)).

$$W_{strong} = \Gamma(W_{concent}; \theta) \tag{1}$$

Here, θ are semantic learned parameters. We expect that the weight transfer function $\Gamma(.)$ is able to transfer coarse semantic information about the appearance of the mitosis to the strong segmentation branch in order to predict a finer mitosis segmentation. We implement $\Gamma(.)$ using a small fully connected network comprising two FC layers, as illustrated in Fig. 3. The FC hidden layer is followed by an activation function of type LeakyReLU. The input of the weight transfer network is $W_{concent}$ while its output is W_{strong}. This weight function is used to tackle the problem of the prediction of the strong segmentation map for images from the dataset without strong annotations in the training stage. It helps transfer the semantic information from the weak predictors to the strong predictors.

C. MODEL TRAINING

We train the concentric segmentation branch using the two-class concentric loss function $L_{concent}$ introduced in [22] on the set $C = A \cup B$, and we train the strong segmentation branch and the weight transfer function $\Gamma(.)$ using a two-class pixel-wise Softmax loss function L_{strong} on the set A only. Thus, the overall loss function of our network is defined as $L = L_{concent} + L_{strong}$.

1) STAGE-WISE TRAINING

Since we use two different segmentation networks, a feasible training strategy is to train the two networks independently. As shown in Fig. 4, we first train the concentric segmentation network using the concentric labels of the set $C = A \cup B$, and then we train the strong segmentation network as well as the weight transfer function using the strong labels of the set A while keeping the convolution features of the concentric segmentation branch unchanged. Thereby, the concentric segmentation weights $W_{concent}$ can be regarded as a fixed embedding vector which does not require any update during the training of the partially supervised segmentation branch.

2) END-TO-END TRAINING

Much of the previous literature on different vision tasks has shown that the multi-task training can yield more accurate results than training on each task independently, such as Mask RCNN [45]. Thus, we propose to jointly train the concentric segmentation branch and the strong segmentation branch of our PartMitosis model in an end-to-end way using the strong and concentric labels of the set A and the concentric labels of the set B, as illustrated in Fig. 5. During the training of the network, $W_{concent}$ will receive gradients from the pixel-wise segmentation loss L_{strong} via the weight transfer function $\Gamma(.)$ only when training with samples from the set A. Hence, directly training the network with back-propagation using the concentric losses on the set $A \cup B$ and the pixel-wise losses on the set A may cause an inconsistency in the concentric segmentation weights $W_{concent}$. Thus, in order to not impede the homogeneity of $W_{concent}$ between the sets A and B, we follow this strategy: when L_{strong} is back-propagated in the network, the gradient of the weights prediction function $\Gamma(W_{concent}; \theta)$ is computed with respect to θ which is the transfer function parameter and stopped with respect to $W_{concent}$, so that the gradient will not be back-propagated to $W_{concent}$. Therefore, $W_{concent}$ will be updated on every training iteration using only the gradient coming from $L_{concent}$ no matter whether the training sample used for this iteration is from the set A or the set B.

D. MODEL INFERENCE

After the training of the PartMitosis model, we apply it to predict two segmentation maps on the breast histological images, as illustrated in Fig. 6. The first segmentation map is denoted by $S_{concent}$, and is the segmentation map produced by the concentric semantic segmentation branch, while the second

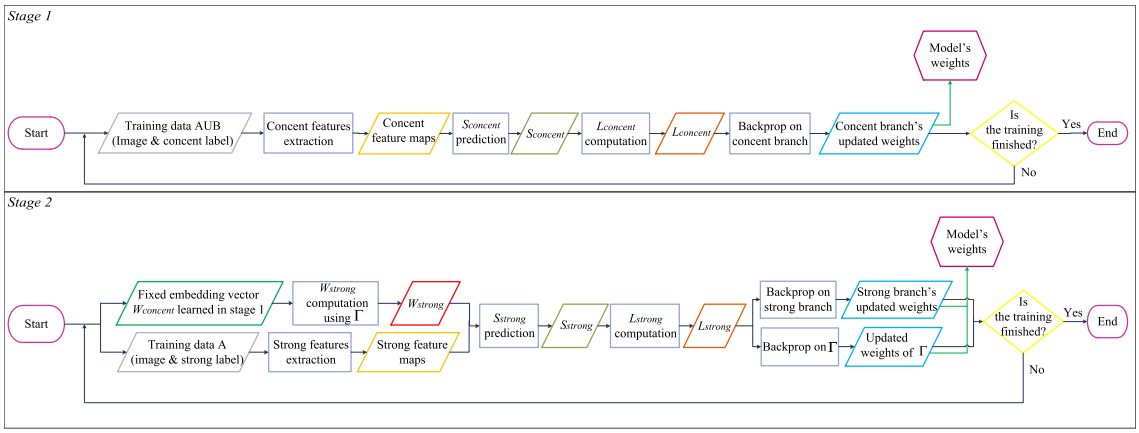

FIGURE 4. Stage-wise training of PartMitosis model.

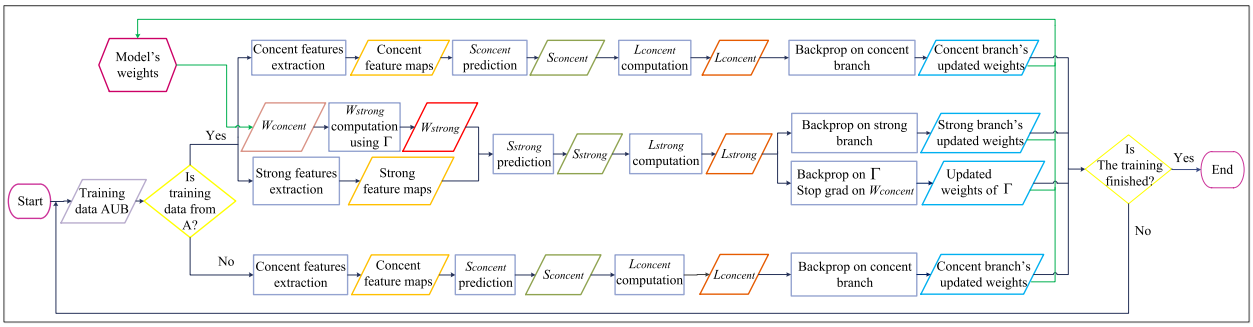

FIGURE 5. End-to-end training of PartMitosis model.

segmentation map, denoted by S_{strong} is the segmentation map generated by the strong semantic segmentation branch. The segmentation map output by each branch contains the probability score of each pixel to be a mitosis. We fuse the concentric score map $S_{concent}$ and the strong score map S_{strong} using Eq. (2)

$$S = w \times S_{concent} + (1 - w) \times S_{strong} \tag{2}$$

We optimize the fusion weight w on the validation set using parameter sweep, i.e., we produce the segmentation maps $S_{concent}$ and S_{strong} for each sample in the validation set, then, for each value of w within the range $[0, 1]$ with a step of 0.1, we produce the fused segmentation maps for all samples in the validation set and then compute the F-score of the model. The weight w that yields the best F-score is used as the model's fusion parameter.

Since the concentric segmentation branch is a coarse segmentation network, it can retrieve the maximum number of existing mitoses. However, because this segmentation network is coarse, it may also retrieve other cells that have appearances almost similar to the mitotic cells. Hence, to remove these false detections, we fuse the coarse predictions with the predictions of the strong segmentation branch. Since the strong branch is a finer segmentation network, because it is trained with strong labels, it can accurately describe the appearance of a mitosis and thus discriminate mitoses from mimics. Fig. 7 shows the advantage of fusing the concentric probability scores with the strong probability scores. In the first example (the first row of Fig. 7), we can see that because the concentric segmentation network is a coarse segmentation network, it can detect more mitotic figures than the strong segmentation branch, so by fusing the score maps of the two networks we can retrieve most of the true mitoses and thus reduce the number of false negatives. In the second example (the second row of Fig. 7), we can see that because the strong segmentation network is a finer segmentation network, it can filter out most of the non-mitotic cells. Hence, by fusing the predicted scores of the two networks, we can eliminate the majority of false mitoses and thus diminish the number of false positives. Therefore, we can conclude that the fusion strategy can exploit the two predicted score maps adequately and achieve more accurate mitosis detection.

The fused prediction map may still contain some noise and tiny ambiguous cells. In order to eliminate them, we propose using the same strategy as in [22], which consists of smoothing the segmentation map by applying a Gaussian filter and then binarizing the filtered map using Otsu's method [46] to obtain segmented blobs. The segmented blobs include mitotic cells as well as some mimic cells. Hence, to filter out false positives, we follow the filtering method

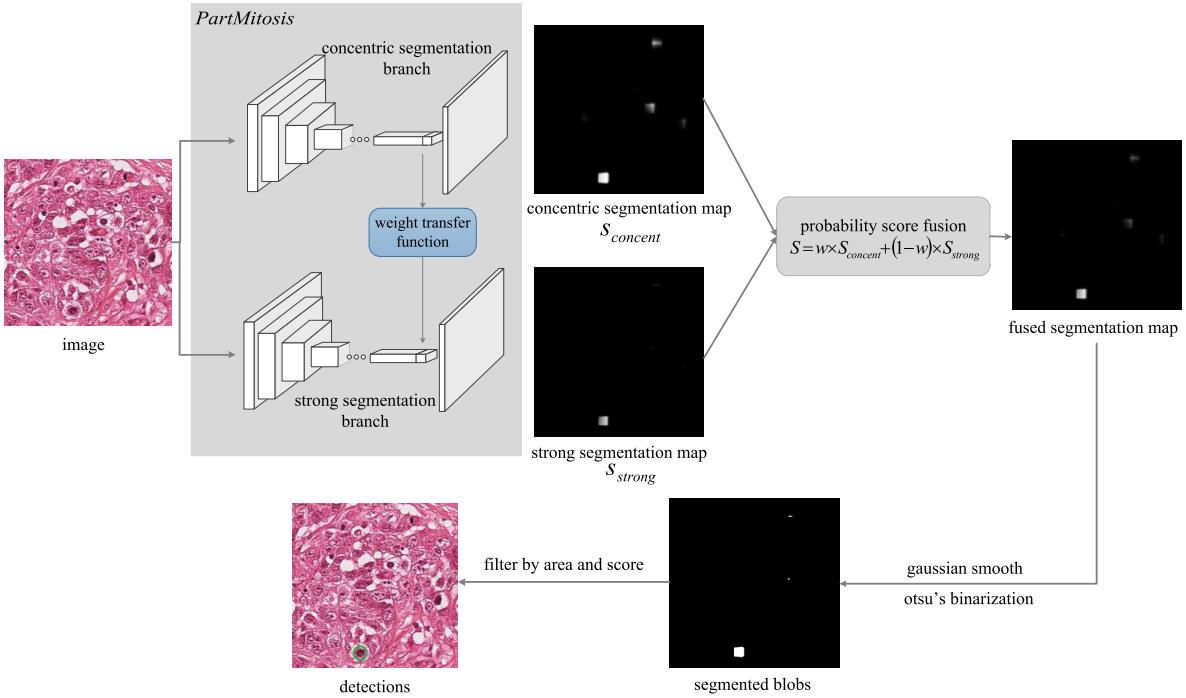

FIGURE 6. Detection of mitotic cells with the PartMitosis model. At inference time, the segmentation map $S_{concent}$ predicted by the concentric segmentation branch is fused with the segmentation map S_{strong} generated by the strong segmentation branch. The fused segmentation map is then smoothed by a Gaussian filter and binarized with Otsu's method to generate the segmented blobs. Finally, filtering by area and confidence score is applied to retrieve the true mitoses and eliminate the false detections. The true detections are represented by the green circles in the final image.

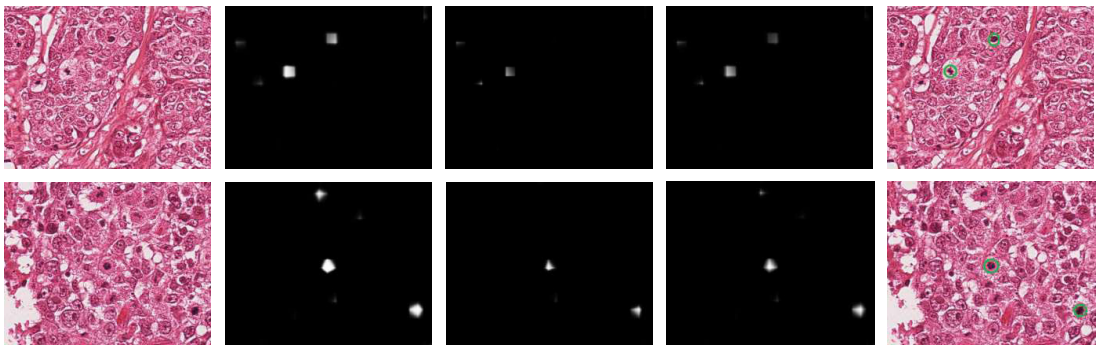

FIGURE 7. Visual impact of fusing the concentric segmentation maps with the strong segmentation maps. (a) Histopathological image samples. (b) Segmentation maps produced by the concentric segmentation branch. (c) Segmentation maps predicted by the strong segmentation branch. (d) Fused segmentation maps. (e) Final mitosis detections after the area and the confidence score filtering. The correct detections are represented by the green circles.

introduced in [22], which eliminates the segmented blobs with a mean score $\bar{S}$ less than a threshold $s1$ or with an area A smaller than a threshold $a1$; otherwise the blob will be kept and considered as a true mitotic cell. As for the weight w, the score threshold $s1$ and the area threshold $a1$ are also optimized on the validation set.

IV. EXPERIMENTS

In this section, we evaluate the performance of our PartMitosis system using three different mitosis datasets, namely: the ICPR 2014 MITOSIS dataset, the AMIDA13 dataset, and the ICPR 2012 MITOSIS dataset.

A. IMPLEMENTATION

The whole PartMitosis system is implemented using the Pytorch framework [47]. We initialized the two segmentation networks of our system with FCN-32s model pre-trained on the Pascal VOC segmentation dataset [48]. We conducted our experiments on a machine with one Nvidia Quadro P5000 GPU.

1) MODEL TRAINING

The training of our PartMitosis system follows the default training strategy of an FCN. Since the two segmentation networks of our framework are based on FCN-32s, i.e., a fully convolutional network with a stride of 32 pixels, we used a learning rate of 1e-10 and set the momentum and the weight decay to 0.99 and 0.0005 respectively. The network was optimized using the stochastic gradient descent method and a batch size of 1. We trained the network for 200k iterations.

2) PERFORMANCE EVALUATION

The evaluation of the performance of a mitosis detection system is based on the number of mitotic cells that are correctly detected. Following the criteria of the mitosis detection contests, if the centroid of a detection is within a certain distance from a ground truth centroid, it is counted as a true mitosis. The distance threshold in the 2012 MITOSIS ICPR dataset is 5 μm (20 pixels), while for the other datasets it is equivalent to 8 μm (32 pixels). The accuracy of the mitosis detection is measured using the F-score, which is given by:

$$F - score = 2 \times recall \times precision/(recall + precision) \tag{3}$$

B. EVALUATION ON THE 2014 MITOSIS DATASET

One of the most challenging mitosis detection datasets is the ICPR 2014 MITOSIS dataset, due to its huge diversity in the appearance and texture of the tissues. As we previously mentioned, to train a PartMitosis model for the detection of mitoses on the 2014 ICPR MITOSIS dataset, we use the training samples of the 2012 MITOSIS dataset as the set A and the training samples from the 2014 MITOSIS dataset as the set B. For the sake of memory, we cropped patches of size 521×521 pixels from the HPF images of the 2012 MITOSIS ICPR training set. We artificially generated more positive patches (patches that contain mitotic cells) using image mirroring, translation in 9 directions, and rotation by 16 angles. For negative patches, we applied image mirroring and rotations in steps of 90 degrees.

We divided the training data of the 2014 ICPR MITOSIS dataset between training and validation in the same way as in [22]: we used the first folder A03 for validation and kept the remaining folders, namely A04, A05, A07, A10, A11, A12 and A14, for training. Hence, the training set contains 534 mitotic cells and the validation set 135. We split each HPF image into patches of 385 × 344 pixels and then augmented the data artificially by applying translation in 9 directions, rotations in steps of 45 degrees, and flipping on positive patches. Since the number of negative patches is already suitable for training our model, we did not apply any augmentation on them.

1) ABLATION EXPERIMENTS

We carried out different ablation experiments with the PartMitosis framework to study the impact of some of its components. We ran these experiments on the 2014 ICPR MITOSIS validation set.

a: IMPACT OF THE END-TO-END TRAINING

We compare the performance results of the PartMitosis model trained in an end-to-end way and the PartMitosis model trained stage-wise to examine the effect of the end-to-end training. We also analyse the impact of disabling the back-propagation of the gradient from L_{strong} to $W_{concent}$ through Γ. As shown in Table 1, the end-to-end training of the PartMitosis model achieves better results than the stage-wise training if only we stop the back-propagation of the gradient of L_{strong} on $W_{concent}$.

TABLE 1. Impact of the training strategy on the 2014 ICPR validation set.

Kind of training	Disabling the gradient on $W_{concent}$	Precision	Recall	F-score
Stage-wise		**0.569**	0.666	0.614
End-to-end		0.529	**0.725**	0.612
End-to-end	×	0.562	0.696	**0.622**

TABLE 2. Impact of the structure of Γ on the 2014 ICPR validation set.

Structure of Γ	Precision	Recall	F-score
1-layer	0.517	0.770	0.619
2-layer, ReLU	0.514	**0.785**	0.621
2-layer, LeakyReLU	**0.562**	0.696	**0.622**
3-layer, ReLU	0.517	0.755	0.614
3-layer, LeakyReLU	0.520	0.740	0.611

b: IMPACT OF THE STRUCTURE OF THE WEIGHT TRANSFER FUNCTION Γ

We investigate the effect of the structure of the weight transfer function Γ on the model's performance by testing different implementations of Γ: a simple affine transformation, a 2-layer Multi-Layer Perceptron (MLP), and a 3-layer MLP. We also tried two types of activation function for the hidden layers: ReLU and LeakyReLU [49]. Table 2 shows the performance results of our PartMitosis model using these different structures of Γ. The best F-score is obtained with the 2-layer neural network and the activation function LeakyReLU.

c: IMPACT OF THE FUSION OF THE CONCENTRIC AND THE STRONG SEGMENTATION MAPS

We also analyse the impact of fusing the probability scores of the concentric segmentation branch and the strong segmentation branch. Fig. 8 shows the change in the performance of the PartMitosis model with respect to the fusion weight w on the validation set. We can see that the PartMitosis model achieves excellent performance when the value of the fusion weight w is 0.6.

2) QUANTITATIVE EVALUATION

Since we split the training data of the 2014 MITOSIS dataset between training and validation in the same way as in the

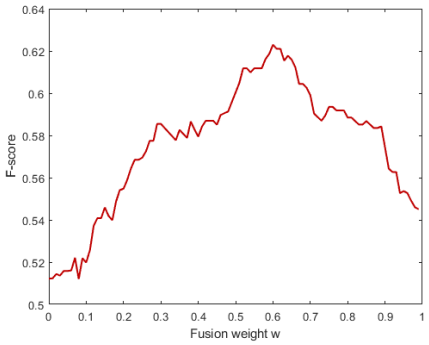

FIGURE 8. The change in the performance of the PartMitosis model with respect to the fusion weight w on the 2014 ICPR validation set.

TABLE 3. Comparison of the performance of the SegMitos models [22] and the PartMitosis models on the 2014 ICPR MITOSIS validation set.

Method	Precision	Recall	F-score
SegMitos-r12R24 [22]	0.516	0.681	0.587
SegMitos-r15R30 [22]	0.495	**0.785**	0.607
SegMitos-random [22]	0.541	0.681	0.603
PartMitosis-r12R24	0.543	0.696	0.610
PartMitosis-r15R30	**0.562**	0.696	**0.622**
PartMitosis-random	0.532	0.674	0.594

SegMitos method, we can compare the performance of PartMitosis to that of SegMitos on the validation set. SegMitos uses three configurations of the concentric label. SegMitos-r12R24 and SegMitos-r15R30 employ a concentric label with two different fixed radii for the small circle r and the large circle R, while SegMitos-random is trained using concentric label with a small radius r randomly selected from the interval $[10, 17]$ and the radius R of the large circle being 1.5 to 2.5 times bigger than r, also randomly chosen. To train the PartMitosis models, we generated random concentric labels for the images of the 2012 MITOSIS training data, while for the 2014 ICPR MITOSIS dataset, we tried the same three concentric label configurations as used for the SegMitos training. Table 3 shows a comparison between the performance of SegMitos and PartMitosis on the 2014 MITOSIS validation set. The PartMitosis models trained with concentric labels of fixed radii achieve better results on the validation set than the SegMitos models trained with the three different concentric label configurations, which demonstrates that with the aid of the proposed weight transfer function, which allows the training of a mitosis detection model in a partially supervised way, we can achieve more accurate detection results for the weakly annotated 2014 ICPR MITOSIS dataset.

We now train the PartMitosis model on all training data (including the validation set) of the 2014 MITOSIS dataset. For the 2014 MITOSIS training samples, we used a concentric label with a small circle r of radius 15 pixels and a large circle R of radius 30 pixels, while for the 2012 MITOSIS training examples we used concentric labels with random radii. We applied the trained model to the 2014 MITOSIS testing set and submitted the mitosis detection results to the challenge organizers. Table 4 and Fig. 9 show the

TABLE 4. Comparison of the performance of PartMitosis with other approaches on the 2014 ICPR MITOSIS testing set. '–' denotes an unreported result.

Method	Precision	Recall	F-score
STRASBOURG [3]	-	-	0.024
YILDIZ [3]	-	-	0.167
MINES-CURIE-INSERM [3]	-	-	0.235
CUHK [3]	0.448	0.300	0.356
MFF-CNN [18]	0.405	0.453	0.428
DeepMitosis [20]	0.431	0.443	0.437
MSSN [19]	0.379	**0.617**	0.470
CasNN(single) [17]	0.411	0.478	0.442
CasNN(average) [17]	0.460	0.507	0.482
SegMitos-r12R24 [22]	0.622	0.463	0.531
SegMitos-r15R30 [22]	0.594	0.512	0.550
SegMitos-random [22]	0.637	0.502	0.562
PartMitosis	**0.664**	0.507	**0.575**

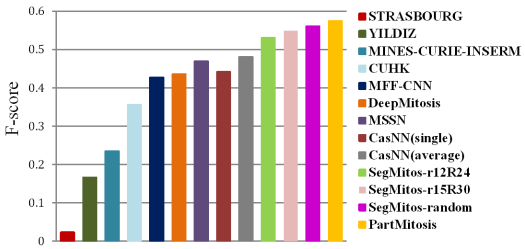

FIGURE 9. Performance comparison of PartMitosis model and other state-of-the-art approaches on the 2014 ICPR MITOSIS testing set.

experimental results of our method and some other previously proposed methods on the 2014 MITOSIS testing set. With an F-score of 0.575, our method outperforms all other approaches, including: STRASBOURG [3], YILDIZ [3], MINES-CURIE-INSERM [3], CUHK [3], which were the 4 winners of the 2014 ICPR MITOS-ATYPIA challenge, MFF-CNN [18], DeepMitosis [20], MSSN [19], CasNN [17] with its two proposed versions, namely the 'single' version that employs only one classification network and the 'average' version that employs three different classification networks and fuses their results, as well as the different configurations of the SegMitos model [22].

3) QUALITATIVE EVALUATION

Fig. 10 shows some samples of the mitosis detections produced by our PartMitosis model on the 2014 ICPR MITOSIS validation set. We can see that almost all of the true mitotic cells are identified by our system, and the mitoses which are not detected are in general extremely small, so it is not evident how to retrieve them. In addition, we can see that the false detections have the same appearance as the true mitoses, hence it is not evident how to screen them out.

C. EVALUATION ON THE AMIDA13 DATASET

To train a PartMitosis model on the AMIDA13 dataset, we converted each HPF image into patches of 500×500 pixels. We augmented the training set by applying translations in 9 directions, rotations in steps of 45 degrees,

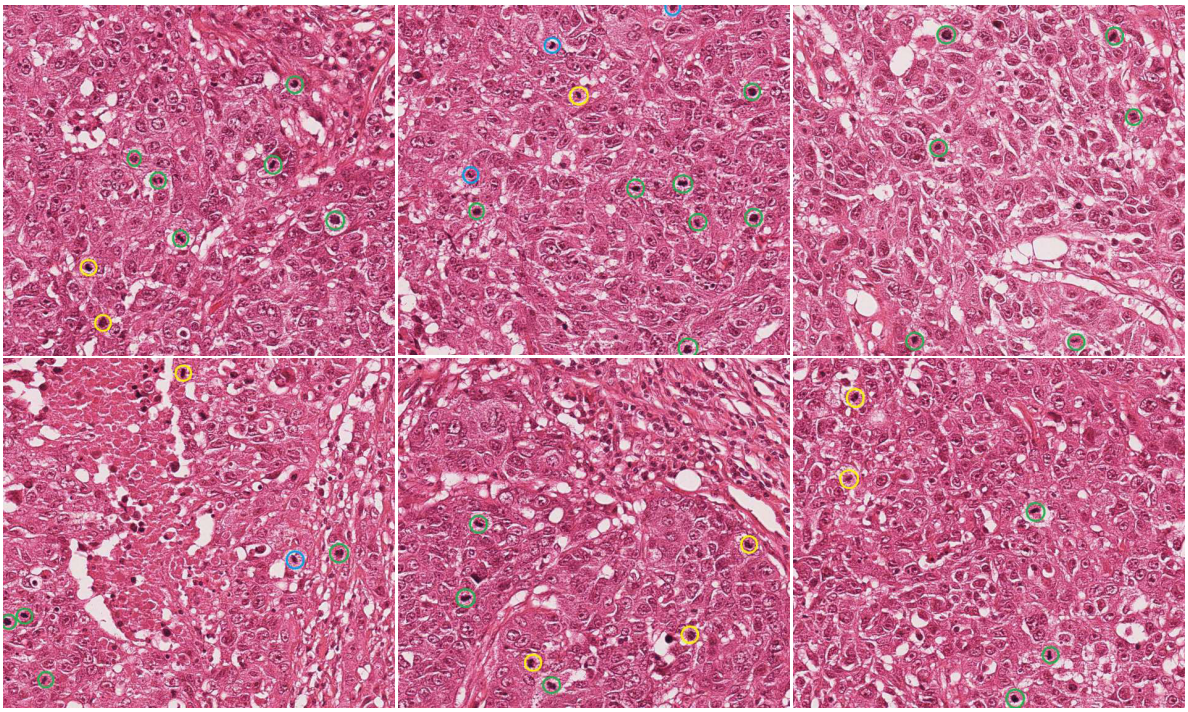

FIGURE 10. Detection results using PartMitosis model on samples from the 2014 ICPR MITOSIS validation set. True positives in green, false negatives in blue, and false positives in yellow.

TABLE 5. Detection performance of PartMitosis model and other approaches on the AMIDA13 testing set.

Method	Precision	Recall	F-score
PANASONIC [4]	0.336	0.310	0.322
ISIK [4]	0.306	0.351	0.327
SURREY [4]	0.357	0.332	0.344
DTU [4]	0.427	0.555	0.483
IDSIA [4]	0.610	0.612	0.611
CUHK [3]	0.690	0.310	0.427
AggNet [50]	0.441	0.424	0.433
SegMitos [22]	0.668	**0.677**	0.672
PartMitosis	**0.743**	0.658	**0.698**

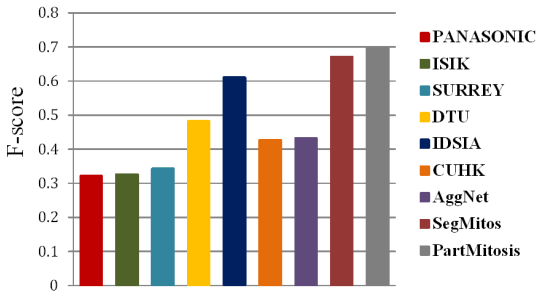

FIGURE 11. Performance comparison of PartMitosis model with other state-of-the-art approaches on the AMIDA13 testing set.

and flipping on positive patches. For negative examples, we only rotated them by 4 angles. For the strongly labeled samples, we used the same augmented 2012 MITOSIS training set that we employed for training the PartMitosis model on the 2014 MITOSIS dataset. The concentric labels were randomly generated for both datasets. The F-scores of our model on the AMIDA13 testing set, as well those of some other approaches, are shown in Table 5 and Fig. 11. The first 5 methods, PANASONIC [4], ISIK [4], SURREY [4], DTU [4] and IDSIA [4], were the top 5 methods that took part in the AMIDA13 challenge. The other three methods, namely CUHK [3], AggNet [50] and SegMitos [22], were methods developed after the challenge. PartMitosis achieves the highest F-score, 0.698, and outperforms all previous methods, including the state-of-the-art SegMitos method. Fig. 12 illustrates some mitosis detections predicted by the PartMitosis model on the AMIDA13 testing set.

D. EVALUATION ON THE 2012 ICPR MITOSIS DATASET

We applied the two PartMitosis models that we trained to detect mitoses in the two weakly annotated mitosis datasets (2014 ICPR MITOSIS dataset and AMIDA13 dataset) to the testing set of the fully annotated 2012 ICPR MITOSIS dataset. The performance results of each PartMitosis model and some other previously proposed methods are shown in Table 6. The best participating methods of the 2012 ICPR MITOSIS contest were the first 4 methods: NEC [13], SUTECH [12], IPAL [6] and IDSIA [15]. As for HC + CNN [14], MSSN [19], CasNN [17], DRN [16], RRF [11], DeepMitosis [20], Improved-mitosis-RCNN [21], and SegMitos-random [22], they were introduced after the challenge. As shown in Table 6, the PartMitosis model that achieves the best F-score on the 2012 MITOSIS testing set is the one trained with the samples from the 2014 MITOSIS

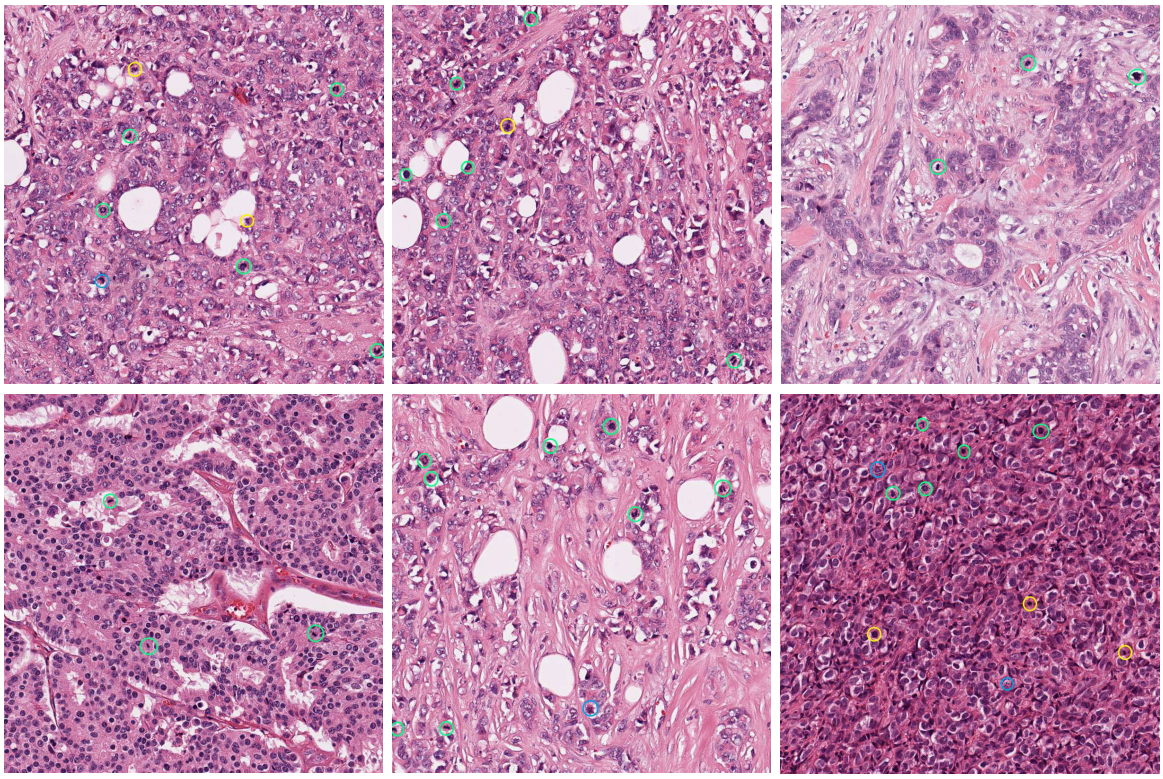

FIGURE 12. Mitosis detections of the PartMitosis method on some image samples from the AMIDA13 testing set. True positives in green, false negatives in blue, and false positives in yellow.

TABLE 6. *F*-scores of PartMitosis models and other methods on the 2012 ICPR MITOSIS testing set.

Method	Precision	Recall	F-score
NEC [13]	0.750	0.590	0.659
SUTECH [12]	0.700	0.720	0.709
IPAL [6]	0.698	0.740	0.718
IDSIA [15]	0.886	0.700	0.782
HC+CNN [14]	0.840	0.650	0.734
MSSN [19]	0.776	0.787	0.781
CasNN [17]	0.804	0.772	0.788
DRN [16]	0.779	0.802	0.790
RRF [11]	0.835	0.811	0.823
DeepMitosis [20]	0.854	**0.812**	0.832
Improved-mitosis-RCNN [21]	**0.920**	0.792	**0.851**
SegMitos-random [22]	0.813	0.732	0.770
PartMitosis-AMIDA13	0.785	0.762	0.773
PartMitosis-MITOSIS2014	0.766	0.811	0.788

dataset and the images from the 2012 MITOSIS dataset: it increases the F-score by 1.8% compared to the SegMitos trained with random concentric labels on the 2012 ICPR MITOSIS dataset. We can also see that the two PartMitosis models obtain more accurate detection results than the SegMitos model. This improvement in performance shows that fusing the scores predicted by the semantic segmentation branch trained with weak labels and the scores produced by the partially supervised segmentation branch trained with strong labels yields better results than considering the probability scores generated by the semantic segmentation model trained with weak labels only, as in the SegMitos method. Some detection results produced by PartMitosis-MITOSIS2014 on images from the 2012 ICPR MITOSIS dataset are shown in Fig. 13.

E. DISCUSSION

It is intriguing that on the two weakly annotated datasets (2014 ICPR MITOSIS dataset and AMIDA13 dataset), our approach leads to better detection results than the previous best method SegMitos [22] and all state-of-the-art methods. Indeed, by achieving F-scores of 0.575 and 0.698 on the 2014 ICPR MITOSIS dataset and AMIDA13 dataset, respectively, our PartMitosis framework improves the mitosis detection performance by 1.3% and 2.6% (in term of F-score) on the 2014 ICPR MITOSIS dataset and AMIDA13 dataset, respectively, compared to the SegMitos method, and surpasses all of the other state-of-the-art approaches by a large margin (more than 9% for the 2014 ICPR MITOSIS dataset and more than 8% for the AMIDA13 dataset). In addition, our method obtains an excellent performance on the fully annotated 2012 ICPR MITOSIS dataset with an F-score of 0.788 and outperforms the SegMitos model trained with the 2012 MITOSIS concentric labels. This improvement in performance is due to the partially supervised learning of our PartMitosis system, which makes mitosis detection more accurate for weakly labeled benchmarks through: (1) Taking advantage of the few available mitosis fully-annotated

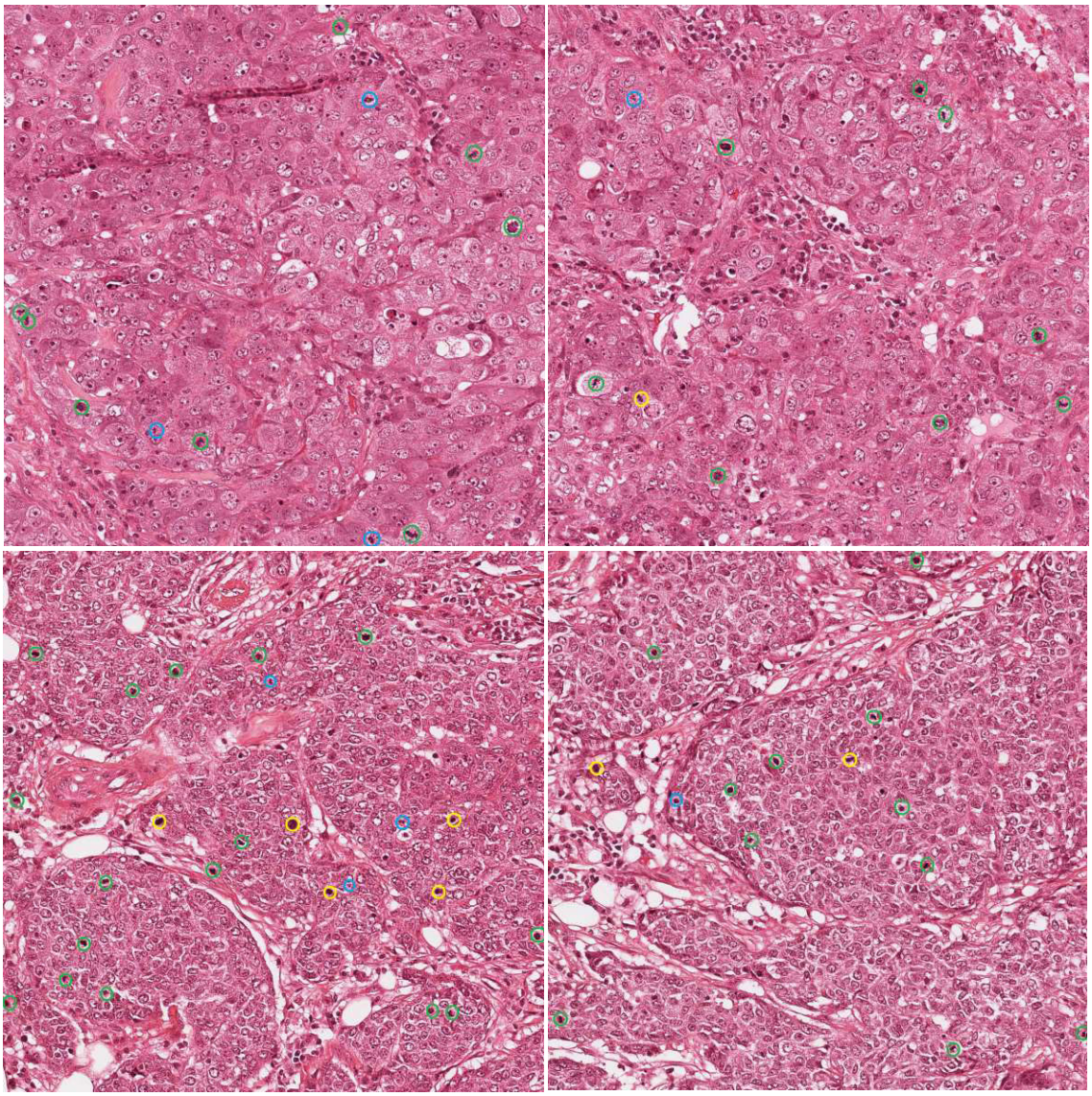

FIGURE 13. Mitoses detected using the PartMitosis-MITOSIS2014 model on some images from the 2012 ICPR MITOSIS testing set. True positives in green, false negatives in blue, and false positives in yellow.

samples and using them on the model's training. (2) Incorporating a weight transfer function that allows the transfer of coarse semantic information from the model's weak predictors to its strong predictors. (3) Fusing the probability score map produced by the weak segmentation branch and the probability score map generated by the strong segmentation branch, which helps to retrieve the largest number of true mitoses and exclude most of the false detections. The state-of-the-art results achieved on the most challenging mitosis detection datasets demonstrate the effectiveness of our PartMitosis system at solving the problem of mitosis detection from histopathological slides with a large weakly annotated dataset and only a small fully labeled dataset.

F. TIME ANALYSIS

Even though our Nvidia Quadro P5000 GPU has 16 GB memory, we cannot process the full HPF image of 2084×2084 pixels from the 2012 ICPR MITOSIS dataset at once since it is still too large to input it into our PartMitosis model. Thus, we cropped patches of 1042×1042 pixels from the full HPF image and fed them into the network. Therefore, it takes about 2.15 s to cut the full image, apply our model to the 4 patches of the HPF image, and put them together to get the full segmentation map. Then, it takes about 0.14 s to obtain the final mitosis detections from the segmentation map. In total, the detection with the PartMitosis system takes about 2.29 s for an image from the 2012 ICPR MITOSIS dataset. The speed of our system is much faster than IDSIA [15], which

takes 31 s to process a 4M-pixel image by a single network and 8 min to fuse multiple detections generated by different models to obtain better results. Our approach is also faster than the state-of-the-art SegMitos [22], which requires 3 s to make detections on the full 2012 MITOSIS image.

For the 2014 ICPR MITOSIS dataset, PartMitosis takes about 1.03 s per 1539 × 1376 HPF, which is slightly greater than the processing time of a 2014 MITOSIS HPF image by the SegMitos [22] model, which requires 0.92 s. The reason behind this is that the SegMitos model is deployed on the full image while our PartMitosis model, for the sake of the GPU memory, is applied to two patches cropped from the full HPF.

V. CONCLUSION

A partially supervised deep learning framework for accurate and reliable mitosis detection from H&E stained histopathological images has been introduced in this paper. We employ a semantic segmentation framework with two-stream fully convolutional networks to segment the breast cancer stained slides. The first branch of the model is trained with weak labels while the second branch is trained with strong labels. We fuse the predicted score maps of the two FCNs to obtain a more accurate mitosis detection. Moreover, we have designed a weight transfer function that can transfer the semantic information from the weak segmentation branch to the strong segmentation branch. This helps tackle the problem of training the strong segmentation branch on a dataset without pixel-level annotations. Our PartMitosis system yields excellent results on the 2012 ICPR MITOSIS dataset, with an F-score of 0.788. In addition, it outperforms all previous methods by achieving F-scores of 0.575 on the 2014 ICPR MITOSIS dataset and 0.698 on AMIDA13 dataset. The excellent results obtained on the most challenging mitosis counting datasets demonstrate the high capacity of our PartMitosis system in mitosis detection and discrimination. In the future, we aim to apply this partially supervised deep learning framework to some other medical applications. Another future investigation is to develop a more sophisticated weight transfer function for a better transfer of learning from one network to another, to improve the mitosis detection performance.

ACKNOWLEDGMENT

The authors would like to thank Dr. X. Wang (an Associate Professor from the School of Electronic Information and Communications, Huazhong University of Science and Technology (HUST), Wuhan, China) for his professional guidance and assistance during the development of this research work and for his comments on the manuscript.

REFERENCES

[1] C. W. Elston and I. O. Ellis, "Pathological prognostic factors in breast cancer. I. The value of histological grade in breast cancer: Experience from a large study with long-term follow-up," *Histopathology*, vol. 19, no. 5, pp. 403–410, Nov. 1991.

[2] L. Roux, D. Racoceanu, N. Loménie, M. Kulikova, H. Irshad, J. Klossa, F. Capron, C. Genestie, G. Naour, and M. Gurcan, "Mitosis detection in breast cancer histological images an ICPR 2012 contest," *J. Pathol. Informat.*, vol. 4, no. 1, p. 8, 2013.

[3] (2014). *MITOS-ATYPIA-14—Grand Challenge, Mitos-Atypia-14-Dataset*. Accessed: Nov. 7, 2019. [Online]. Available: https://mitos-atypia-14.grand-challenge.org/dataset/

[4] M. Veta *et al.*, "Assessment of algorithms for mitosis detection in breast cancer histopathology images," *Med. Image Anal.*, vol. 20, no. 1, pp. 237–248, 2015.

[5] C. Sommer, L. Fiaschi, F. A. Hamprecht, and D. W. Gerlich, "Learning-based mitotic cell detection in histopathological images," in *Proc. 21st Int. Conf. Pattern Recognit. (ICPR)*, 2012, pp. 2306–2309.

[6] H. Irshad, "Automated mitosis detection in histopathology using morphological and multi-channel statistics features," *J. Pathol. Informat.*, vol. 4, no. 1, p. 10, 2013.

[7] F. Tek, "Mitosis detection using generic features and an ensemble of cascade adaboosts," *J. Pathol. Informat.*, vol. 4, no. 1, p. 12, 2013.

[8] A. M. Khan, H. El-Daly, and N. M. Rajpoot, "A gamma-Gaussian mixture model for detection of mitotic cells in breast cancer histopathology images," in *Proc. 21st Int. Conf. Pattern Recognit. (ICPR)*, 2012, pp. 149–152.

[9] C. H. Huang and H. K. Lee, "Automated mitosis detection based on exclusive independent component analysis," in *Proc. 21st Int. Conf. Pattern Recognit. (ICPR)*, 2012, pp. 1856–1859.

[10] M. Veta, P. J. Van Diest, and J. P. W. Pluim, "Detecting mitotic figures in breast cancer histopathology images," *Proc. SPIE*, vol. 8676, Mar. 2013, Art. no. 867607.

[11] A. Paul, A. Dey, D. P. Mukherjee, J. Sivaswamy, and V. Tourani, "Regenerative random forest with automatic feature selection to detect mitosis in histopathological breast cancer images," in *Proc. Int. Conf. Med. Image Comput. Comput. Assist. Interv.*, 2015, pp. 94–102.

[12] A. Tashk, M. S. Helfroush, H. Danyali, and M. Akbarzadeh, "An automatic mitosis detection method for breast cancer histopathology slide images based on objective and pixel-wise textural features classification," in *Proc. 5th Conf. Inf. Knowl. Technol.*, May 2013, pp. 406–410.

[13] C. Malon and E. Cosatto, "Classification of mitotic figures with convolutional neural networks and seeded blob features," *J. Pathol. Informat.*, vol. 4, no. 1, p. 9, 2013.

[14] H. Wang, A. Cruz-Roa, A. Basavanhally, H. Gilmore, N. Shih, M. Feldman, J. Tomaszewski, F. Gonzalez, and A. Madabhushi, "Cascaded ensemble of convolutional neural networks and handcrafted features for mitosis detection," *Proc. SPIE*, vol. 9041, Mar. 2014, Art. no. 90410.

[15] D. C. Cireşan, A. Giusti, L. M. Gambardella, and J. Schmidhuber, "Mitosis detection in breast cancer histology images with deep neural networks," in *Proc. Int. Conf. Med. Image Comput. Comput. Assist. Interv.*, 2013, pp. 411–418.

[16] H. Chen, X. Wang, and P. A. Heng, "Automated mitosis detection with deep regression networks," in *Proc. IEEE 13th Int. Symp. Biomed. Imag. (ISBI)*, Apr. 2016, pp. 1204–1207.

[17] H. Chen, Q. Dou, X. Wang, J. Qin, and P. A. Heng, "Mitosis detection in breast cancer histology images via deep cascaded networks," in *Proc. 30th AAAI Conf. Artif. Intell.*, 2016, pp. 1160–1166.

[18] T. Kausar, M. Wang, B. Wu, M. Idrees, and B. Kanwal, "Multi-scale deep neural network for mitosis detection in histological images," in *Proc. Int. Conf. Intell. Informat. Biomed. Sci. (ICIIBMS)*, Oct. 2018, pp. 47–51.

[19] M. Ma, Y. Shi, W. Li, Y. Gao, and J. Xu, "A novel two-stage deep method for mitosis detection in breast cancer histology images," in *Proc. 24th Int. Conf. Pattern Recognit. (ICPR)*, Aug. 2018, pp. 3892–3897.

[20] C. Li, X. Wang, W. Liu, and L. J. Latecki, "DeepMitosis: Mitosis detection via deep detection, verification and segmentation networks," *Med. Image Anal.*, vol. 45, pp. 121–133, Apr. 2018.

[21] H. Lei, S. Liu, H. Xie, J. Y. Kuo, and B. Lei, "An improved object detection method for mitosis detection," in *Proc. 41st Annu. Int. Conf. IEEE Eng. Med. Biol. Soc. (EMBC)*, Jul. 2019, pp. 130–133.

[22] C. Li, X. Wang, W. Liu, L. J. Latecki, B. Wang, and J. Huang, "Weakly supervised mitosis detection in breast histopathology images using concentric loss," *Med. Image Anal.*, vol. 53, pp. 165–178, Apr. 2019.

[23] R. Hu, P. Dollar, K. He, T. Darrell, and R. Girshick, "Learning to segment every thing," in *Proc. IEEE/CVF Conf. Comput. Vis. Pattern Recognit.*, Jun. 2018, pp. 4233–4241.

[24] A. Krizhevsky, I. Sutskever, and G. E. Hinton, "Imagenet classification with deep convolutional neural networks," in *Proc. Adv. Neural Inf. Process. Syst.*, 2012, pp. 1097–1105.

[25] K. Simonyan and A. Zisserman, "Very deep convolutional networks for large-scale image recognition," 2014, *arXiv:1409.1556*. [Online]. Available: http://arxiv.org/abs/1409.1556

[26] C. Szegedy, W. Liu, Y. Jia, P. Sermanet, S. Reed, D. Anguelov, D. Erhan, V. Vanhoucke, and A. Rabinovich, "Going deeper with convolutions," in *Proc. IEEE Conf. Comput. Vis. Pattern Recognit. (CVPR)*, Jun. 2015, pp. 1–9.
[27] K. He, X. Zhang, S. Ren, and J. Sun, "Deep residual learning for image recognition," in *Proc. IEEE Conf. Comput. Vis. Pattern Recognit. (CVPR)*, Jun. 2016, pp. 770–778.
[28] P. Tang, X. Wang, Z. Huang, X. Bai, and W. Liu, "Deep patch learning for weakly supervised object classification and discovery," *Pattern Recognit.*, vol. 71, pp. 446–459, Nov. 2017.
[29] K. Nguyen, C. Fookes, A. Ross, and S. Sridharan, "Iris recognition with off-the-shelf CNN features: A deep learning perspective," *IEEE Access*, vol. 6, pp. 18848–18855, 2017.
[30] P. Liu, H. Zhang, W. Lian, and W. Zuo, "Multi-level wavelet convolutional neural networks," *IEEE Access*, vol. 7, pp. 74973–74985, 2019.
[31] R. Girshick, J. Donahue, T. Darrell, and J. Malik, "Rich feature hierarchies for accurate object detection and semantic segmentation," in *Proc. IEEE Conf. Comput. Vis. Pattern Recognit.*, Jun. 2014, pp. 580–587.
[32] R. Girshick, "Fast R-CNN," in *Proc. IEEE Int. Conf. Comput. Vis. (ICCV)*, Dec. 2015, pp. 1440–1448.
[33] S. Ren, K. He, R. Girshick, and J. Sun, "Faster R-CNN: Towards real-time object detection with region proposal networks," in *Proc. Adv. Neural Inf. Process. Syst.*, 2015, pp. 91–99.
[34] J. Wang, X. Wang, and W. Liu, "Weakly- and semi-supervised faster R-CNN with curriculum learning," in *Proc. 24th Int. Conf. Pattern Recognit. (ICPR)*, Aug. 2018, pp. 2416–2421.
[35] A. Rohan, M. Rabah, and S.-H. Kim, "Convolutional neural network-based real-time object detection and tracking for parrot AR drone 2," *IEEE Access*, vol. 7, pp. 69575–69584, 2019.
[36] O. Ronneberger, P. Fischer, and T. Brox, "U-net: Convolutional networks for biomedical image segmentation," in *Proc. Int. Conf. Med. Image Comput. Comput. Assist. Interv.*, Nov. 2015, pp. 234–241.
[37] L.-C. Chen, G. Papandreou, I. Kokkinos, K. Murphy, and A. L. Yuille, "DeepLab: Semantic image segmentation with deep convolutional nets, atrous convolution, and fully connected CRFs," *IEEE Trans. Pattern Anal. Mach. Intell.*, vol. 40, no. 4, pp. 834–848, Apr. 2018.
[38] K. C. Santosh, N. Alam, P. P. Roy, L. Wendling, S. Antani, and G. R. Thoma, "A simple and efficient arrowhead detection technique in biomedical images," *Int. J. Pattern Recognit. Artif. Intell.*, vol. 30, no. 5, Apr. 2016, Art. no. 1657002.
[39] K. C. Santosh, L. Wendling, S. Antani, and G. R. Thoma, "Overlaid arrow detection for labeling regions of interest in biomedical images," *IEEE Intell. Syst.*, vol. 31, no. 3, pp. 66–75, May 2016.
[40] K. C. Santosh and P. P. Roy, "Arrow detection in biomedical images using sequential classifier," *Int. J. Mach. Learn. Cybern.*, vol. 9, no. 6, pp. 993–1006, 2018.
[41] S. Khan, N. Islam, Z. Jan, I. Ud Din, and J. J. P. C. Rodrigues, "A novel deep learning based framework for the detection and classification of breast cancer using transfer learning," *Pattern Recognit. Lett.*, vol. 125, pp. 1–6, Jul. 2019.
[42] A. Hatamizadeh, D. Terzopoulos, and A. Myronenko, "End-to-End boundary aware networks for medical image segmentation," in *Proc. Int. Workshop Mach. Learn. Med. Imag.*, 2019, pp. 187–194.
[43] J. Long, E. Shelhamer, and T. Darrell, "Fully convolutional networks for semantic segmentation," in *Proc. IEEE Conf. Comput. Vis. Pattern Recognit. (CVPR)*, Jun. 2015, pp. 3431–3440.
[44] N. Tajbakhsh, J. Y. Shin, S. R. Gurudu, R. T. Hurst, C. B. Kendall, M. B. Gotway, and J. Liang, "Convolutional neural networks for medical image analysis: Full training or fine tuning?" *IEEE Trans. Med. Imag.*, vol. 35, no. 5, pp. 1299–1312, May 2016.
[45] K. He, G. Gkioxari, P. Dollar, and R. Girshick, "Mask R-CNN," in *Proc. IEEE Int. Conf. Comput. Vis. (ICCV)*, Oct. 2017, pp. 2961–2969.
[46] N. Otsu, "A threshold selection method from gray-level histograms," *IEEE Trans. Syst., Man, Cybern.*, vol. SMC-9, no. 1, pp. 62–66, Jan. 1979.
[47] A. Paszke, S. Gross, S. Chintala, G. Chanan, E. Yang, Z. DeVito, Z. Lin, A. Desmaison, L. Antiga, and A. Lerer, "Automatic differentiation in PyTorch," in *Proc. NIPS*, 2017, pp. 1–4.
[48] M. Everingham, L. Van Gool, C. K. I. Williams, J. Winn, and A. Zisserman, "The Pascal visual object classes (VOC) challenge," *Int. J. Comput. Vis.*, vol. 88, no. 2, pp. 303–338, 2010.
[49] A. L. Maas, A. Y. Hannun, and A. Y. Ng, "Rectifier nonlinearities improve neural network acoustic models," in *Proc. Int. Conf. Mach. Learn. (ICML)*, 2013, vol. 30, no. 1, p. 3.
[50] S. Albarqouni, C. Baur, F. Achilles, V. Belagiannis, S. Demirci, and N. Navab, "AggNet: Deep learning from crowds for mitosis detection in breast cancer histology images," *IEEE Trans. Med. Imag.*, vol. 35, no. 5, pp. 1313–1321, May 2016.

MERIEM SEBAI received the B.S. and M.S. degrees from the University of Science and Technology Houari Boumediene (USTHB), Algiers, Algeria, in 2014 and 2016, respectively. She is currently pursuing the Ph.D. degree with the School of Computer Science and Technology, Huazhong University of Science and Technology (HUST), Wuhan, China. Her research interests include image processing, medical image analysis, machine learning, and deep learning.

TIANJIANG WANG received the Ph.D. degree from the Huazhong University of Science and Technology (HUST), Wuhan, China, in 2002. He is currently a Professor with the School of Computer Science and Technology, HUST. His research interests include artificial intelligence, machine learning, computer vision, and image processing.

SAAD ALI AL-FADHLI received the B.Sc. degree in computer science from the University of Baghdad and the M.Sc. degree in computer science from Pune University, Pune, India, in 2012. He is currently pursuing the Ph.D. degree in IoT systems design and security with the Huazhong University of Science and Technology, China. From July 2013 to July 2017, he was a Lecturer with the Imam Al-Kadhum College, Najaf, Iraq. His research interests include the IoT and VANET systems design and security.